Separating Solvent and Conformational Effects on the Photophysics of a Homologous Progression of N-Terminated Phenylenevinylene Oligomers

ARTICLE *in* THE JOURNAL OF PHYSICAL CHEMISTRY C · AUGUST 2013

Impact Factor: 4.77 · DOI: 10.1021/jp406048g

THE JOURNAL OF PHYSICAL CHEMISTRY C

Article

pubs.acs.org/JPCC

Separating Solvent and Conformational Effects on the Photophysics of a Homologous Progression of N-Terminated Phenylenevinylene Oligomers

Telma Costa,*[,†,‡] Roberto E. Di Paolo,[§] Logan E. Garner,[‡] Alexander W. Thomas,[‡] João A. S. Almeida,[†] Licínia L.G. Justino,[†,⊥] António L. Maçanita,[§] Guillermo C. Bazan,[‡] and Hugh D. Burrows[†]

[†]Chemistry Department, University of Coimbra, 3004-535 Coimbra, Portugal

[‡]Center for Polymers and Organic Solids, Department of Physics and Chemistry & Biochemistry, University of California, Santa Barbara, California 93106, United States

[§]Centro de Química Estrutural, Instituto Superior Técnico, Technical University of Lisbon, 1049-001 Lisbon, Portugal

[⊥]Centro de Neurociências e Biologia Celular, Universidade de Coimbra, Portugal

S *Supporting Information*

ABSTRACT: A homologous series of *p*-phenylenevinylene oligomers $(PPV)_n$ (n = 3−5) with terminal dialkylamino groups have been synthesized, and characterized. The photophysical and solvatochromic properties of oligomers with three, four, and five phenyl groups were investigated in solution through steady-state and time-resolved fluorescence. The red-shift seen in absorption and photoluminescence (PL) spectra on increasing chain length is consistent with an extension of the conjugation length. Decreasing solvent polarity leads to small shifts of the absorption spectra and large blue-shifts of the PL spectra. Time-resolved emission on these oligomers allows separation of conformational and solvent contributions to their photophysical behavior. Global analysis of fluorescence decays collected at different emission wavelengths shows biexponential behavior in toluene at room temperature. The longer time appears as a decay component at all emission wavelengths and decreases from 949 to 850 ps with increasing chain length. The shorter time component (19−26 ps) appears as a decay at the onset of the emission spectrum and as a rise time at longer wavelengths. With PPV oligomers substituted on the phenyl rings, similar kinetic characteristics have been attributed to conformational relaxation of the initially excited oligomer into a more planar conjugation. However, the solvent and temperature dependence exclude this hypothesis. Instead, this component is assigned to specific interaction between the oligomer main chain and the solvent. Information on backbone conformational behavior has been obtained by temperature dependence of multinuclear NMR studies coupled with molecular dynamics simulations, Møller−Plesset 2, and density functional theory (DFT) calculations. The major result is that conformational relaxation in the excited state can be decoupled from solvent relaxation. Since conformational relaxation enhances nonradiative decay, control of this is expected to improve photoluminescence yields in these systems.

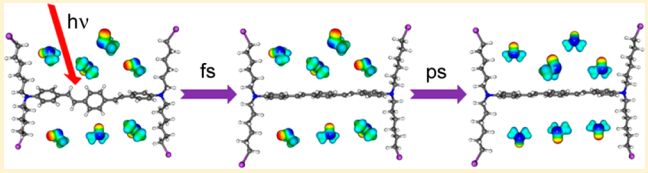

1. INTRODUCTION

Conjugated organic polymers are playing a major role in the developing field of plastic electronics because of their applications in light-emitting diodes (LEDs), thin film transistors, photovoltaic devices, and sensors.[1−5] Potential advantages of organic over inorganic semiconductors are their low cost, versatility of chemical synthesis, easy processing, and possibilities of producing flexible devices.[6−10] A major topic of research interest involves understanding the optical and electronic properties of conjugated polymers (CP) in relation to the wide range of polymer structures. Furthermore, control of macromolecular organization and chain conformation are extremely important for obtaining the optimal performance in optoelectronic devices. Although these materials are normally used as thin films, they are cast from solutions, and film morphology and optical properties are strongly dependent on their solution structure. The quality of the solvent is a parameter that has to be considered in order to control the solution structure of these polymers. For example, poly[9,9-dioctylfluorene-2,7-diyl] (PFO) has shown different structural features in good (toluene) and in poor (methylcyclohexane) solvents.[11] In toluene, PFO forms one-dimensional elongated structures composed of individual chains, whereas in methylcyclohexane larger aggregates with a planar geometry (sheetlike structures) are formed.

para-Phenylenevinylene (PPV) polymers and oligomers are one of the most important classes of conjugated materials.[12] The olefinic bonds connecting the benzene rings limit the twisting on the backbone thus limiting conformational freedom and,

Received: June 19, 2013
Revised: August 2, 2013
Published: August 2, 2013

consequently, increasing the effective conjugation length of the polymer segments.[13] A rigid and planar ladder structure can easily be achieved in these polymers and oligomers. Poly[2,5-bis(diethylaminetetraethylene glycol) phenylene vinylene] (DEATG-PPV) adopts different chain conformations depending on the solvent.[14] When DEATG-PPV is dissolved in chloroform, methanol, and water, it is seen to assume an extended polymer chain conformation, a coiled chain conformation, and a collapsed chain conformation, respectively. With the important poly(2-methoxy-5-(2′ethylhexyl)oxy-1,4-phenylene vinylene) (MEH-PPV) in methyltetrahydrofuran, a transition is observed on cooling from a relatively disordered defect cylinder conformation to a more extended and more ordered one.[15] Thus DEATG-PPV gives rise to regular chain packing and moderate-to-weak interchain interaction in the lamellae structure obtained from the evaporation of a good solvent, chloroform, while relatively smooth film morphology is observed in methanol-processed films, and closely packed aggregates are obtained from water, giving rise to small-sized and bright aggregates.[14] In addition, conjugated polymer film morphology can be modified *a postiori* by solvent vapor annealing (SVA).[16] Although questions remain about the actual mechanisms of SVA, there is no doubt that polymer−solvent interactions are involved.

A valuable approach to investigate the influence of solvent interactions on polymeric organic semiconductors is to study the corresponding conjugated oligomers (COs) which are simpler to synthesize and which are monodisperse. These are described in terms of a small number of repeat units containing an electronically π-delocalized backbone. In addition, if these contain electron-donating end-groups, the donor−acceptor−donor structure introduces useful spectroscopic features, such as large-two-photon absorption cross sections.[17] Although these systems do not formally possess a molecular dipole, the two-photon absorption arises because of the quadrupolar distribution of electron density leading to solvatochromic properties. These are expected to be temperature dependent because of backbone conformational changes.

In this contribution, we report on three homologous *p*-phenylenevinylene oligomers capped at both ends with dialkylamino pendant groups (Scheme 1) and the effect of the solvent and temperature on their photophysical properties under very dilute solution conditions where interchromophore interactions are absent. The alkyl chains are terminated by iodo groups as the oligomers are precursors in synthesis of water-soluble compounds produced via quaternization. However, this is not expected to change the photophysical behavior of the oligomers. To help understand the role of conformation on their behavior, we have also carried out NMR spectral studies accompanied by computational studies and molecular dynamics simulations.

Scheme 1. Structure of the Neutral Oligomers (COs)

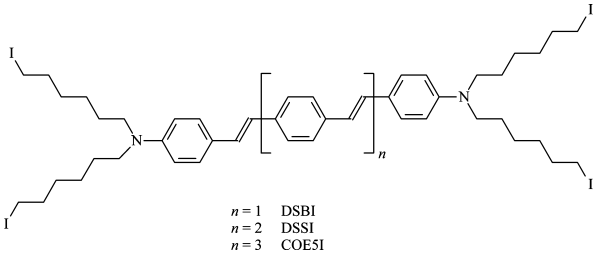

2. RESULTS

2.1. Photophysical Properties of COs. *Photophysics in Toluene.* The absorption and photoluminescence (PL) spectra of the three oligomers DSBI, DSSI, and COE5I in toluene (a good solvent for the COs, see Materials, Methods, and Techniques) are presented in Figure 1a. The absorption spectra show poorly resolved vibronic structure, and their maxima shift to longer wavelengths with increasing oligomer length. The PL spectra in toluene are vibronically resolved, and the emission maxima are also red-shifted by ca. 23 nm from the trimer to the tetramer and ca. 9 nm from the tetramer to the pentamer (Table 1).

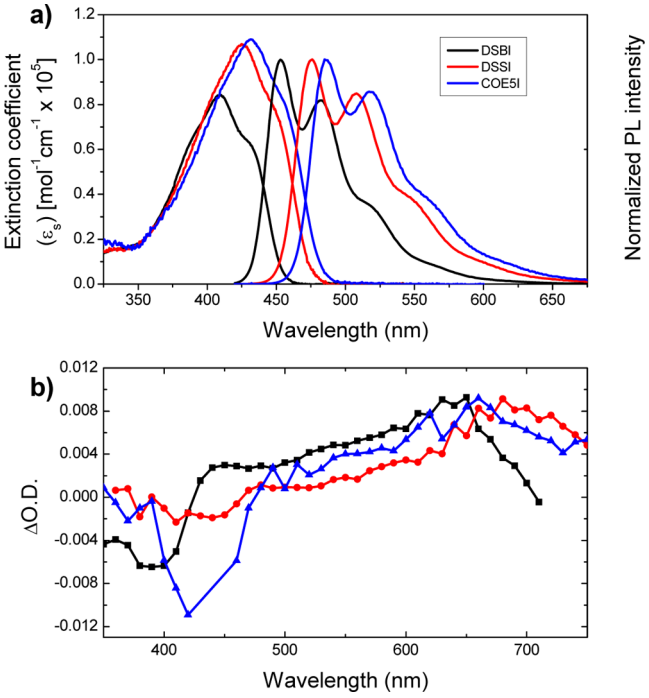

Figure 1. (a) Absorption and PL spectra (excitation at maxima absorption wavelength) and (b) transient absorption spectra of DSBI, DSSI, and COE5I, in toluene, at room temperature. The transient absorption spectra were obtained following the excitation at 355 nm (abs at 355 nm ~0.25) and with a delay after flash of 16 μs.

The triplet state of the oligomers has been characterized through laser flash photolysis and their propensity for singlet oxygen formation. From these experiments, it has been possible to determine the triplet absorption maxima (λ_T), extinction coefficients (ε_T), and triplet (ϕ_T) and singlet oxygen (ϕ_Δ) quantum yields, see Table 1. The transient triplet−triplet absorption spectrum for the trimer is similar to those reported for a related system[18,19] and shows depletion of the ground-state absorption between 350 and 500 nm and a broad absorption band ranging from 500 to 800 nm (Figure 1b) suggesting some delocalization of the excited triplet state.[20] The transient triplet−triplet absorption spectra of the three oligomers are similar and have a maximum in the range of 650−680 nm. A second, poorly resolved band is observed with DSBI and DSSI at 450 and 480 nm, respectively. This follows somewhat different kinetic behavior. While we have not been able to attribute this, a similar band has been observed with other *p*-phenylenevinylene trimers.[21]

Although singlet oxygen and triplet state quantum yields of conjugated polymers are frequently very similar,[22] with the oligomers the ϕ_Δ values appear to be about half ϕ_T. However, from both sets of values, triplet-state formation is only a relatively

dx.doi.org/10.1021/jp406048g | J. Phys. Chem. C 2013, 117, 18353−18366

Table 1. Spectral Data: Absorption (λ_{abs}) and Fluorescence (λ_{em}) Wavelength Maxima, Triplet−Triplet Absorption (λ_T) Maxima, and Extinction Singlet (ε_S) and Triplet (ε_T) Coefficients. Photophysical Properties: Fluorescence Quantum Yields (ϕ_F), Intersystem Crossing Singlet-to-Triplet Quantum Yields (ϕ_T), Quantum Yields for Singlet Oxygen Formation (ϕ_Δ), Fluorescence Lifetimes (τ_f), Radiative (k_f), Radiationless Internal Conversion (k_{IC}), and Intersystem Crossing (k_{ISC}) Rate Constants of DSBI, DSSI, and COE5I, in Toluene, at 293 K

compound	λ_{abs} nm	ε_S mol^{-1} cm^{-1}	λ_T nm	ε_T mol^{-1} cm^{-1}	λ_{em} nm	ϕ_F[a]	ϕ_T	ϕ_Δ	τ_f ps	k_f[b] ns^{-1}	k_{IC}[c] ns^{-1}	k_{ISC}[d] ns^{-1}
DSBI	409	8.42×10^4	650	6.4×10^3	453	0.77	0.08	0.042	947	0.81	0.16	0.08
DSSI	426	10.7×10^4	680	5.4×10^3	476	0.72	0.1	0.053	899	0.80	0.20	0.11
COE5I	431	10.9×10^4	660		485	0.64			850	0.75	0.42	

[a] ϕ_F values were measured relative to a fluorescein standard at pH 12. [b] $k_f = \phi_f/\tau_f$. [c] $k_{IC} = (1 - \phi_f - \phi_T)/\tau_f$. [d] $k_{ISC} = \phi_T/\tau_F$.

minor photophysical pathway, and the ε_T, ϕ_T, and ϕ_Δ values are essentially constant for DSBI and DSSI.

Both the ϕ_F and τ_F decrease slightly with an increase of the number of rings as a consequence of the decrease and increase of, respectively, the radiative (k_f) and the sum of nonradiative (k_{nr}) rate constants. The increase in nonradiative deactivation results in part from an increase in internal conversion. As we will discuss later, this may be due, at least in part, to increasing conformational flexibility on increasing chain length.

The fluorescence decays of DSBI, DSSI, and COE5I in toluene were collected with picosecond time resolution at the beginning, maximum, and tail of their emission bands. In this solvent, the three oligomers show biexponential decays, with a short component of 19−26 ps (τ_1) and a long component of 850−949 ps (τ_2), depending on the oligomer (Table 2).

Table 2. Decay Times (τ_i) and Pre-Exponential Coefficients (A_i) Derived from Global Analysis of Fluorescence Decays of DSBI, DSSI, and COE5I, in Toluene at 20 °C, Measured at Three Emission Wavelengths[a]

oligomer	λ_{exc} (nm)	λ_{em} (nm)	τ_1 (ps)	τ_2 (ps)	A_1	A_2	χ^2
		440			0.28	0.72	1.09
DSBI	423	480	19	949	0.06	0.94	0.88
		500			−0.10	1	0.94
		460			0.32	0.68	0.99
DSSI	420	490	25	899	−0.13	1	1.44
		520			−0.15	1	0.87
		465			0.38	0.62	0.96
COE5I	442	515	26	850	0.09	0.91	0.99
		575			−0.02	1	1.01

[a] Reduced chi-squared values (χ^2) are also shown.

The pre-exponential coefficient of the longer decay component (τ_2) is always positive across the emission band and is assigned to the lifetime of the relaxed oligomer, which decreases with increasing chain length. The shorter time component (τ_1) appears as a decay time at the onset of the emission band and as a rise time at the end. Similar short components have been observed in related systems, and various explanations have been given.[6,23] These include on-chain energy transfer, solvent relaxation, and conformational relaxation[24−26] depending on the systems under investigation. With the oligomers, on-chain energy transfer is unlikely. To distinguish between the other two possibilities and to establish the most probable mechanism for the rise time at longer wavelengths, we have examined the temperature effect on the spectra (shown in the Supporting Information, SI) and decay times. Decay times and pre-exponential coefficients obtained from global analysis, for DSBI in toluene in the −70 to 70 °C temperature range, are depicted in Figure 2a. Shown as an inset the temperature effect is presented on the steady-state PL spectra.

The longest decay time (τ_2) increases on lowering the temperature, whereas the shortest decay time remains constant within experimental error over the range of temperatures studied ($\tau_1 \sim$ 19−24 ps). The negative pre-exponential associated with the shortest component becomes slightly more negative at 540 nm with decreasing temperature (Figure 2d), whereas at 490 nm the opposite effect is observed (Figure 2c). At −30 °C, a third component with a decay time of 295 ps appears and gradually decreases to 136 ps at −70 °C. This intermediate decay time might be either due to aggregation or to a nonrelaxed conformation adopted by the oligomer at low temperatures. This species predominantly emits at the blue edge of the emission spectrum, and at the longer wavelength, the pre-exponential factor has very low amplitude.

The same pattern was observed for the other two conjugated oligomers in toluene (data not shown), including the absence of temperature dependence for the shortest decay time (see Figure S7 of the SI), which indicates that it cannot be due to conformational relaxation.

Solvent Effect on the Photophysics of COs. The PL spectra of the three oligomers show high sensitivity to the solvent, namely, very large red-shifts and complete loss of vibrational resolution in high polarity solvents as illustrated in Figure 3a, b, and c for DSBI, DSSI, and COE5I, respectively. The solvent-induced red-shift is less pronounced in the absorption spectra of the three oligomers (Table 3) leading to large Stokes shifts, which indicate substantial differences between the equilibrium structures of ground and excited states.

Previous studies with DSBI and its derivatives[27] have assigned these large shifts and loss of vibronic structure to intramolecular charge transfer (ICT) from the electron-rich dialkylamino groups to the conjugated framework. It has been shown that the increase of the acceptor character of the internal ring gives rise to a more pronounced ICT in the excited state and larger changes in the emission spectra by solvent stabilization.[27]

The ICT nature of the lowest energy transition was analyzed with the Lippert−Mataga eq 1,[28] which predicts a linear dependence of the Stokes shift $\Delta\upsilon(\Delta\upsilon = \upsilon_{abs} - \upsilon_{ems})$ on the Lippert polarity/polarizability function $\{\Delta f = [(\varepsilon - 1)/(2\varepsilon + 1)] - [(n^2 - 1)/(2n^2 + 1)]\}$ with slope proportional to the change in the dipole moment upon excitation $(\Delta\mu = \mu_E - \mu_G)$ and to the reciprocal third power of the Onsager radius, a.

$$\Delta\upsilon = \frac{2}{hc} \times \frac{(\mu_E - \mu_G)^2}{a^3} \times \Delta f + \text{const} \quad (1)$$

From the Lippert−Mattaga plots for DSBI, DSSI, and COE5I (Figure 4), a linear dependence of the Stokes shift with the solvent polarizability is found for all solvents supporting the importance of solvent reorganization/relaxation around the excited state.

dx.doi.org/10.1021/jp406048g | J. Phys. Chem. C 2013, 117, 18353−18366

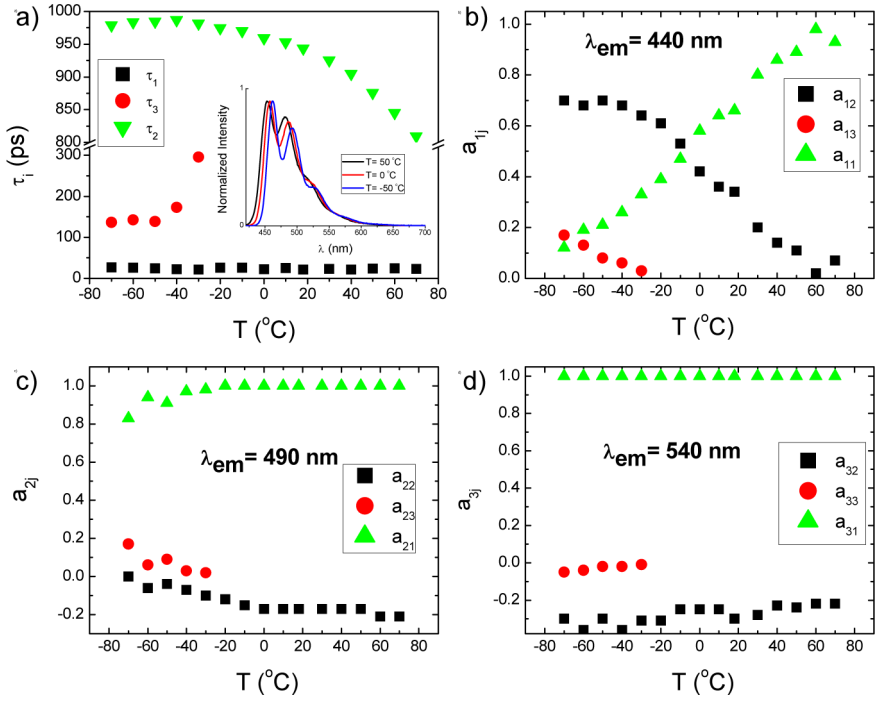

Figure 2. (a) Decay times (τ_i) and pre-exponential coefficients at (b) 440 nm (a_{1j}), (c) 490 nm (a_{2j}), and (d) 540 nm (a_{3j}) of DSBI in toluene as a function of temperature. Shown as an inset are the normalized PL spectra of DSBNI, in toluene, at 50, 0, and −50 °C.

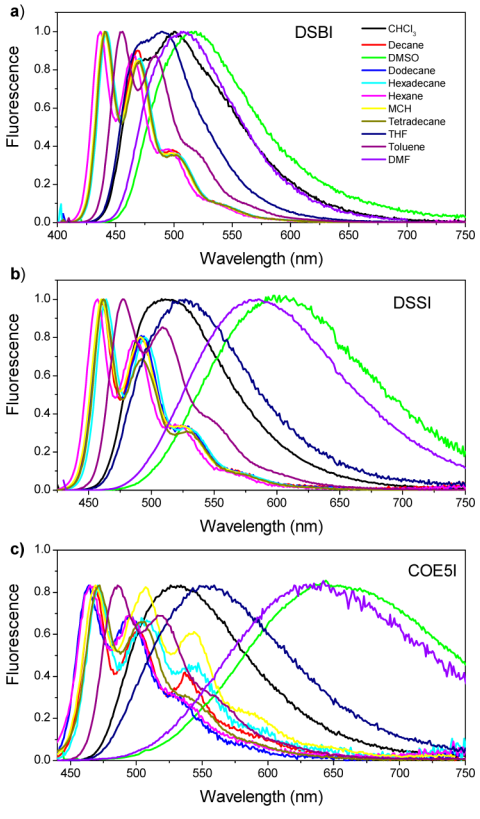

Figure 3. PL spectra of (a) DSBI, (b) DSSI, and (c) COE5I in different solvents at room temperature.

The Lippert−Mattaga plots reveal large dipole moment changes (12.5, 16.1, and 18.0 D for DSBI, DSSI, and COE5I, respectively) upon excitation. These large dipole moments are in agreement with the highest occupied molecular orbital (HOMO) → lowest unoccupied molecular orbital (LUMO) transition having intramolecular charge-transfer character. While the substituted distyrylbenzenes are effectively symmetric and should have zero dipole moment, the charge-transfer transition involves the dialkylamino groups leading to the observed change.

From MP2 calculations (Figure S1 of the SI), the spatial distributions of HOMO and LUMO show that the HOMO level is uniformly delocalized over the entire oligomer (amino nitrogens and the *p*-phenylenylene units), whereas the LUMO is mainly located on the central rings.

Information on charge transfer can also be obtained using empirical solvent parameters; with these oligomers, an approximately linear relationship was observed between the empirical $E_T(30)$ polarity parameter and the $\Delta\upsilon$ (Figure S2 of the SI) in agreement with charge transfer and differential solvation of the ground and excited states.[29]

The fluorescence decays of the three oligomers were measured with ps time resolution at the onset, middle, and tail of the emission band in solvents with different polarities and viscosities. In nonpolar solvents (*n*-hexane, methylcyclohexane (MCH), and *n*-hexadecane), the decays were single exponentials with decay times in the 890−970 ps time range. In polar solvents, from toluene to dimethylsulfoxide (DMSO), the decays became double or triple exponentials with a fast component ranging from 8 to 19 ps. The pre-exponential coefficient of the fast component decreases with increasing emission wavelength and becomes negative (rise time) at longer wavelengths as found in toluene. Table 4 shows the decay times and pre-exponential coefficients obtained for DSBI (fluorescence decays for the three oligomers are given in the SI).

From inspection of Table 4, it is clear that the fast component observed in polar solvents is not correlated with the solvent viscosity. The independence from solvent viscosity is in complete agreement with the previous indication resulting from temperature studies that the fast component is not associated with torsional relaxation to a more planar conformation of the

dx.doi.org/10.1021/jp406048g | J. Phys. Chem. C 2013, 117, 18353−18366

Table 3. Maximum Absorption (λ_{abs}) and Emission (λ_{em}) Wavelengths in nm of DSBI, DSSI, and COE5I in Different Solvents

				DSBI			DSSI			COE5I		
solvent	ε^a	$n_D{}^{b\ 58}$	$\eta^{c\ 58}$(mPa.s)	λ_{abs}	λ_{em}	$\Delta\lambda^d$	λ_{abs}	λ_{em}	$\Delta\lambda^d$	λ_{abs}	λ_{em}	$\Delta\lambda^d$
hexane	1.89	1.375	0.313	399	437	38	413	457	47	405	467	62
decane	1.99	1.411	0.928	401	440	39	417	460	43	422	469	47
dodecane	2.01	1.422	1.508	402	441	39	420	462	42	419	464	45
tetradecane	2.03	1.429	2.342	403	441	38	420	462	42	423	471	48
hexadecane	2.05	1.434	3.351	404	442	38	420	462	42	424	471	47
MCH	2.02	1.423	0.734	402	440	38	417	460	43	425	469	55
toluene	2.38	1.497	0.586	410	456	46	425	477	52	432	486	54
chloroform	4.81	1.490	0.58	407	475[e]	68	426	512	86	433	529	98
				407	501	94						
THF	7.68	1.404	0.48	410	472[e]	62	427	527	100	434	554	120
				410	490	80						
DMF	36.7	1.431	0.92	415	508	93	433	583	150	437	637	200
DMSO	47.2	1.479	1.996	419	516	97	436	602	166	443	650	207

[a]Dieletric constant. [b]Refractive index. [c]Viscosity. [d]$\Delta\lambda = \lambda_{em} - \lambda_{abs}$. [e]Shoulder at the emission band.

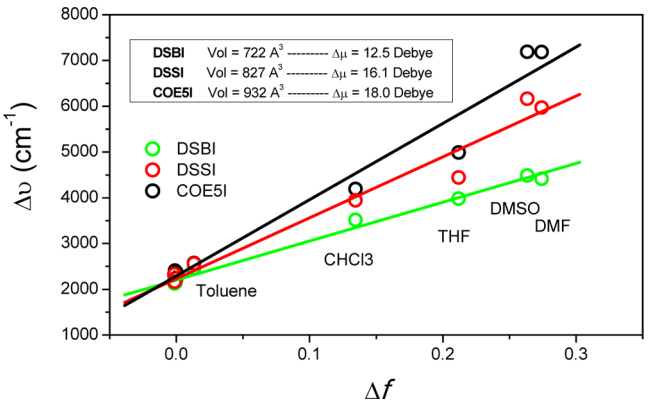

Figure 4. Lippert–Mataga plots of DSBI, DSSI, and COE5I in the different solvents indicated in Table 3 at room temperature.

oligomer in the excited state.[30] This is further supported by the observed invariance with temperature of the shorter time of DSBI and DSSI also in the polar solvent chloroform (Figure S7 of the SI).

The foregoing conclusion contrasts with that observed for *p*-phenylenevinylene trimers possessing alkoxyl side-chain groups on the aromatic rings, where torsional relaxation, occurring in tens of picoseconds, was observed.[24] Because the marked Stokes shift and the increase in vibronic structure of the PL compared with the absorption spectra of the present oligomers show that conformational relaxation must occur, this relaxation must happen on a subpicosecond time scale.[31] Therefore, we have measured fluorescence decays of DSBI in MCH at the onset (430 nm) and at the tail (520 nm) of the emission band with femtosecond time resolution using fluorescence up-conversion (Figure 5). As expected, the decays clearly showed a subpicosecond (894 fs) component appearing as a decay time at the band onset and as a rise time at the longer wavelenth.

The 980 fs time is substantially shorter than the viscosity dependent conformational relaxation times of distyrylbenzenes substituted with alkoxyl groups on the aromatic rings:[24] 24 and 37 ps for, respectively, methylbutyloxyl (MBOPV3) and ethylhexyloxyl (EHOPV3) side chains in MCH at 293 K. Actually, the much shorter fast component for DSBI is the result expected from the effect of van der Waals (VdW) volume of the side chains on the relaxation time shown in Figure 6:[25] the relaxation time decreases with the decrease of the VdW volume of side or terminal chains. A detailed theoretical description of this effect and its quantitative application to the interpretation of the data in Figure 6 has been recently published.[32]

Nelson et al. have presented a realistic scenario for the ultrafast photoinduced dynamics of distyrylbenzene using nonadiabatic excited-state molecular dynamics simulations.[33] Conformational relaxation involving partial planarization of the backbone was predicted to occur on a 100 fs time scale at 300 K. This theoretical value is significantly lower than the 980 fs measured by us for DSBI in MCH, which was also expectable from the presence of the dialkylamino terminal groups of DBSI and from the absence of terminal and side-chain groups in distyrylbenzene. The 980 fs lifetime lies in between the 100 fs value for distyrylbenzene and the reported conformational relaxation times of distyrylbenzenes substituted with alkoxyl groups on the aromatic rings.[24] Thus, we tentatively assign the 980 fs decay to torsional relaxation, which, as noted earlier, may be one of the processes favoring internal conversion. Further fluorescence up-conversion studies of solvent viscosity and temperature effects on the relaxation time will be carried out for a definitive assignment of this process.

2.2. NMR Spectroscopy and Theoretical Calculations on Conformational Behavior. NMR spectroscopy provides an excellent tool for understanding the ground-state conformational behavior of the conjugated oligomers since chemical shifts are sensitive to molecular orbital distribution and, consequently, to the structure and bonding of the molecule.[34] This allows correlation of NMR chemical shifts with oligomer conformations for different solvents and temperatures. Figure 7 presents the ^{13}C and ^{1}H NMR spectra and the assignment of all the resonances of DSSI in $CDCl_3$. Ambiguities in the assignment were resolved through COSY, HETCOR, DEPT, and ROESY experiments. A comparison between the chemical shift values in chloroform-*d* and in toluene-d_8 is given in Table S1 of the SI.

To obtain an insight into the structures of DSBI, DSSI, and COE5I, we have optimized the geometries of this series of oligomers at the B3LYP/6-31G(d,p) and MP2/3-21G(d) levels. Model systems, where the $C_6H_{12}I$ substituents at the nitrogen atoms were replaced by ethyl moieties, were used to reduce the computation time. The density functional theory (DFT) minimum energy geometries for the series of oligomers differ strongly from the MP2/3-21G(d) geometries particularly concerning the backbone dihedral angles. While the DFT structures show dihedral angles between the planes of the

dx.doi.org/10.1021/jp406048g | J. Phys. Chem. C 2013, 117, 18353–18366

Table 4. Decay Times (τ_i) and Pre-Exponential Coefficients (A_i) Resulting from Global Analysis of the Decays of DSBI in Solvents with Different Viscosities (η) and Relative Dielectric Constants (ε)

solvent	η (cP)	ε[58]	λ_{exc} (nm)	λ_{em} (nm)	τ_1 (ps)	τ_2 (ps)	τ_3 (ps)	A_1	A_2	A_3	χ^2
				430					1.00		1.17
n-hexane	0.313	1.89	380	470		892			1.00		0.90
				510					1.00		0.95
				440					1.00		1.18
n-hexadecane	3.351	2.05	423	470		969			1.00		1.53
				540					1.00		0.96
				430					1.00		1.14
MCH	0.734	2.02	380	470		894			1.00		1.07
				510					1.00		1.03
				440				0.28	0.72		1.09
toluene	0.586	2.38	423	480	19	949		0.06	0.94		0.88
				500				−0.10	1		0.94
				450				0.52	0.47	0.01	1.08
chloroform	0.563	4.81	415	490	15	935	1582	−0.02	0.93	0.07	1.05
				570				−0.39	0.50	0.50	0.98
				450				0.40	0.60		0.95
THF	0.48	7.68	412	480	8	1081		0.14	0.86		1.00
				540				−1	1		0.95
				455				0.71	0.29		1.10
DMF	0.924	36.7	412	510	8	1280		−0.04	1		0.97
				600				−0.80	1		1.04
				470				0.54	0.40	0.06	0.99
DMSO	1.996	47.2	390	510	14	1226	1882	0.12	0.74	0.14	1.01
				590				−0.41	0.70	0.30	1.01

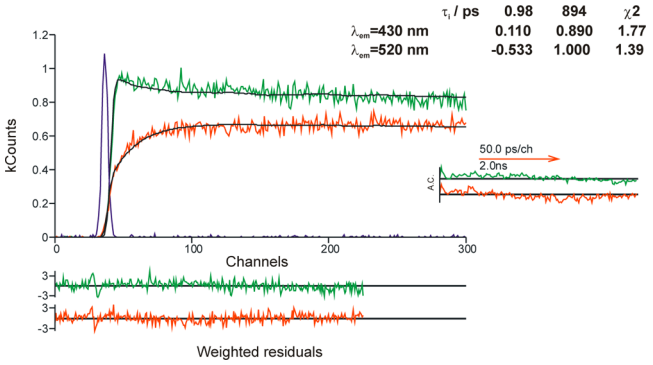

Figure 5. Global analysis of the fluorescence decays of DSBI in MCH measured at the onset (430 nm) and tail (520 nm) of the emission band with fluorescence up-conversion. The longer decay time was fixed equal to the value obtained from TCSPC (894 ps). The resulting decay times (τ_i) and pre-exponential coefficients (A_i) are shown as well as the fit parameters: reduced chi-squared values (χ^2), weighted residuals (WR), and autocorrelation functions (AC). The Instrumental Response Function (IRF) is shown in blue.

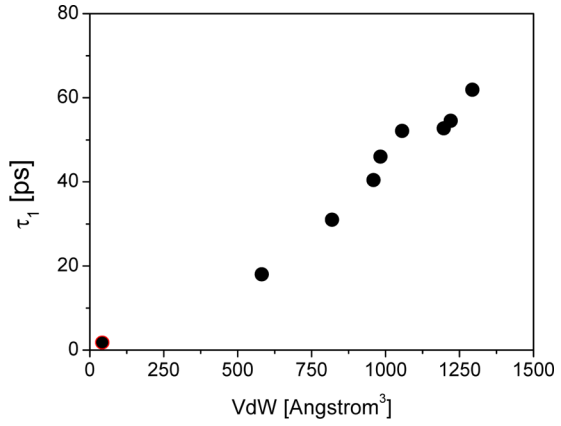

Figure 6. Relaxation times of MBOPV3, EHOPV3, and six abietic acid-based amine-end-capped *p*-phenylenevinylene trimers in toluene at 293 K vs the van der Waals volume of side chains plus end-capped groups. DSBI in MCH is included taking for the VdW volume the sum of VdW volumes of the six hydrogens.

successive phenyl and vinylene units varying from 0.28 to 6.92 degrees, the MP2 structures have dihedral angles varying from 25.54 to 29.44 degrees. Additionally, the DFT calculations for the series of oligomers indicate, as expected, that as the number of monomer units increases, both the HOMO and the LUMO stabilize and the energy of the optical gap decreases.

Since NMR spectroscopy is sensitive to very small electronic changes, the calculation of NMR chemical shifts and the comparison with the experimental values provides a stringent test for evaluating how close the theoretical structures are to the actual structures in solution. Therefore, we have calculated the ^{13}C NMR chemical shifts for the DFT and the MP2 geometries of DSSI using the B3LYP/GIAO method and have compared them with the experimental chemical shifts of DSSI at −30 and 55 °C. Table 5 summarizes the results. From the calculated chemical shifts, the MP2 structure seems to be in better agreement with the experimental solution structure of DSSI. In particular, the C(5)/C(18), C(6)/C(17), C(7)/C(16), C(10)/C(13), and C(11)/C(12) ^{13}C chemical shifts are much better reproduced from the MP2 structure and support the idea that the solution structure is not planar.

Semiempirical PM6 and molecular dynamics (MD) results agree in suggesting dihedral angles between the planes of the successive phenyl and vinylene units of the same magnitude but give values that are higher than those obtained by MP2/3-21G. Table 6 summarizes the geometrical parameters obtained using the different calculation methods, while Figure 8 shows the MP2/3-21G(d) optimized geometries of the model systems

dx.doi.org/10.1021/jp406048g | J. Phys. Chem. C 2013, 117, 18353−18366

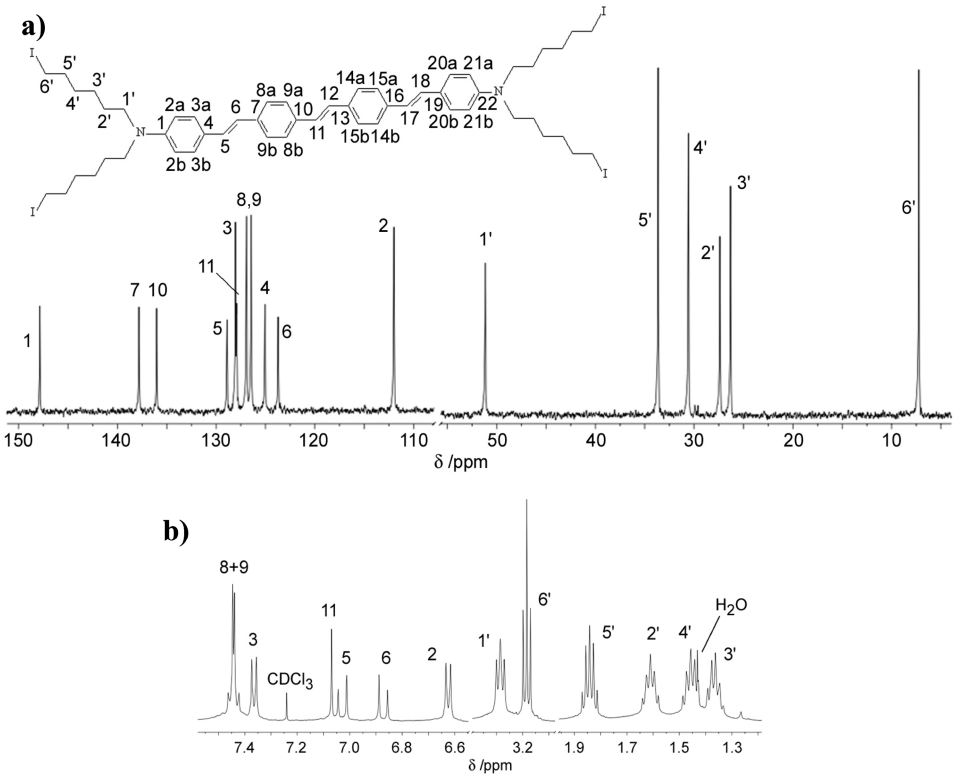

Figure 7. (a) ^{13}C NMR and (b) ^{1}H NMR spectra of a 0.02 M DSSI solution in $CDCl_3$ at 298.15 K.

Table 5. Comparison Between the Backbone ^{13}C NMR Experimental Chemical Shifts of the Tetramer DSSI in $CDCl_3$ at 243.15 and 328.15 K and the Calculated Values for the B3LYP/6-31G(d,p) and the MP2/3-21G(d) Structures in Vacuum[a]

site	MP2/3-21G(d)	B3LYP/6-31G(d,p)	expt −30 °C	expt 55 °C
C(1)/C(22)	142.35	140.75/140.74	147.13	148.24
C(2a)/C(21b)	110.28	108.41/108.33	111.11	112.51
C(2b)/C(21a)	109.08	107.74/107.50	111.11	112.51
C(3a)/C(20b)	122.51	119.64/119.63	127.91	128.10
C(3b)/C(20a)	126.91	127.36/127.54	127.91	128.10
C(4)/C(19)	125.81	123.14/122.85	124.02	125.62
C(5)/C(18)	129.97	124.69/124.38	128.42	129.13
C(6)/C(17)	124.36	118.73/118.35	122.93	124.14
C(7)/C(16)	138.60	134.48/134.39	137.35	138.04
C(8a)/C(14b)	126.23	126.27/126.32	126.77/126.22[b]	127.01/126.56[b]
C(8b)/C(14a)	125.82	126.25/126.28	126.77/126.22[b]	127.01/126.56[b]
C(9a)/C(15b)	121.35	117.93/117.91	126.22/126.77[b]	126.56/127.01[b]
C(9b)/C(15a)	122.30	118.04/118.03	126.22/126.77[b]	126.56/127.0[b]
C(10)/C(13)	136.82	132.20/132.17	135.47	136.30
C(11)/C(12)	129.17	122.74/122.81	127.40	128.19

[a]Numbering refers to Figure 7a. [b]Possibility of a reverse assignment.

(the semiempirical PM6 optimized structures are shown in Figure S4 of the SI).

Molecular dynamics (MD) were also used to simulate the conformational behavior. Nonunimodal distributions of small dihedral angles (predominantly below 30 degrees) between the planes of the successive phenyl and vinylene units were obtained from MD at 273 K (data not shown) suggesting that a variety of similar conformations can coexist. However, interconversion between conformations occurs as a consequence of simultaneous changes in several angles with it becoming impossible to get them isolated from the MD trajectory. On increasing the temperature for MD simulations to 298 K, unimodal distributions of relatively larger angles (between 30 and 60 degrees as presented in Table 6) were obtained. Rigidity of these residues was also verified by MD through monitoring the end-to-end distance between the N atoms for each molecule at 273 K and 298 K. Results are depicted in Figure S5 of the SI. From this analysis, it is clear that all the molecules under study have a limited ability to bend with these distances remaining almost constant along the simulation runs. For DSBI, it is also apparent that temperature has a negligible influence on this parameter, while for DSSI and COE5I a reduced distance is observed for the higher temperature. The effect of the temperature is more important in the latter case, where the shorter distance is compatible with a larger bending of the global structure. Combination of MD, MP2, and PM6

dx.doi.org/10.1021/jp406048g | J. Phys. Chem. C 2013, 117, 18353−18366

Table 6. Dihedral Angles between the Plans of the Successive Phenyl and Vinylene Units Calculated using MP2/3-21G(d), PM6 Semiempirical, and MD (298 K) for the Trimer, Tetramer, and Pentamer

	trimer			tetramer			pentamer		
φ (degrees)	MP2/3-21G(d)	PM6	MD	MP2/3-21G(d)	PM6	MD	MP2/3-21G(d)	PM6	MD
$\varphi 1$	25.75	40.22	34.80	25.63	40.33	56.34	25.89	39.46	42.15
$\varphi 2$	29.13	41.09	50.30	29.29	40.73	58.07	28.78	41.62	50.51
$\varphi 3$	29.15	41.10	49.71	29.11	41.57	56.17	26.08	40.81	47.99
$\varphi 4$	25.78	40.19	56.19	29.08	40.47	60.72	27.71	40.84	36.01
$\varphi 5$				29.28	41.73	37.65	27.52	40.83	34.13
$\varphi 6$				25.54	40.80	55.75	26.91	40.74	34.59
$\varphi 7$							29.44	41.72	39.08
$\varphi 8$							25.55	40.73	41.86

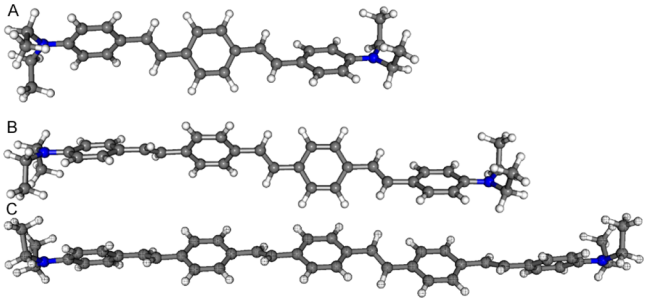

Figure 8. MP2/3-21G(d) optimized geometries of model systems of (a) trimer (DSBI), (b) tetramer (DSSI), and (c) pentamer (COE5I). The $C_6H_{12}I$ substituents at the nitrogen atoms were replaced by ethyl moieties. The inputs for optimization were built considering planar backbones and trans conformations of the ethyl groups.

calculations suggests that the main conformational processes involve changes in torsional angles along the chains.

To obtain further insight into the conformational behavior of DSSI, a variable temperature NMR study was carried out in the interval from −30 °C to +55 °C. Figures 9 and 10 show the ^{13}C and ^{1}H NMR spectra and the chemical shift changes for each resonance ($\Delta\delta$ values). The ^{13}C resonances of all the aromatic carbon atoms of DSSI undergo a downfield shift ($\Delta\delta > 0$) with the increase in temperature from −30 °C to +55 °C (Figure 9). Similarly, the ^{1}H chemical shifts of DSSI vary with temperature; however, both downfield and upfield shifts are observed for the backbone protons making the ^{1}H spectral modifications more difficult to analyze (Figure 10). These changes of the ^{13}C and ^{1}H chemical shifts are in agreement with changes in the population of different conformational states and suggest that the temperature dependence of the PL excitation spectra in Figure 3a must be due, at least in part, to changes in ground-state conformation.

To survey the conformational stability and to interpret the chemical shift variation with temperature, a model of the backbone of DSSI was considered, and its energy and ^{13}C nuclear magnetic shielding constants were computed by MP2 and DFT calculations as a function of the relevant dihedral angles. Figure 11 presents this analysis. The DFT calculations on the model of Figure 11a indicate an energy minimum close to 0 degrees for $\varphi 1$ and $\varphi 2$ dihedrals and a second minimum, lower in energy, close to 180 degrees (this agrees with the almost planar geometries obtained for the series of oligomers by DFT). As expected, the MP2 calculations on the model indicate for $\varphi 1$ and $\varphi 2$ a minimum close to 30 degrees and a second minimum, slightly higher in energy, close to 150 degrees, in agreement with the structure obtained for the tetramer at MP2 level.

The ^{13}C nuclear magnetic shielding constant dependence with the dihedral angle is shown in Figure 11b. The results are shown for the C7, C8, C9, C10, and C14 carbon atoms as a function of the dihedral angle $\varphi_1(10, 9, 8, 7)$. For this calculation, only the MP2/3-21G(d) geometries of the model of Figure 11 with varying dihedral angle were considered. The selected carbon atoms are representative (in terms of chemical environment) of the majority of carbon atoms in the backbone of DSSI. From

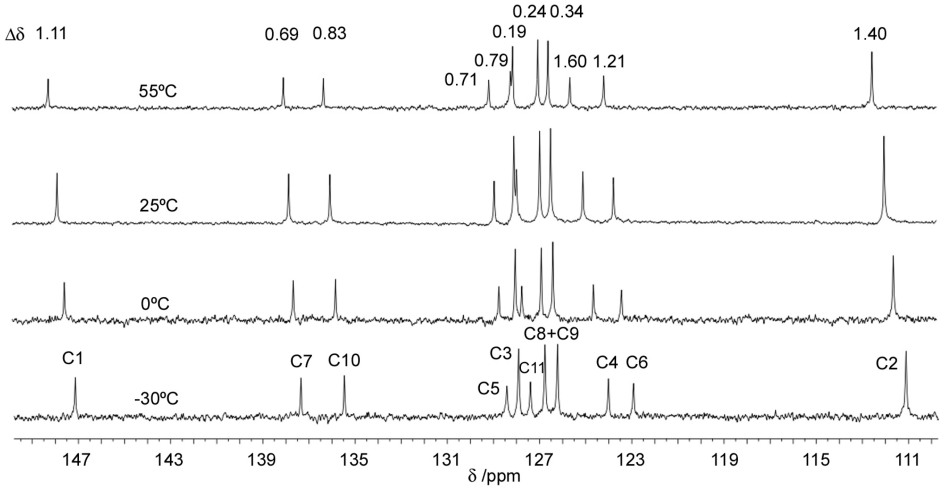

Figure 9. Expanded view of the aromatic region of the ^{13}C NMR spectra of a 0.02 M DSSI solution in $CDCl_3$ at indicated temperatures and $\Delta\delta$ values defined as $\Delta\delta = \delta_{55\ °C} - \delta_{-30\ °C}$.

dx.doi.org/10.1021/jp406048g | J. Phys. Chem. C 2013, 117, 18353−18366

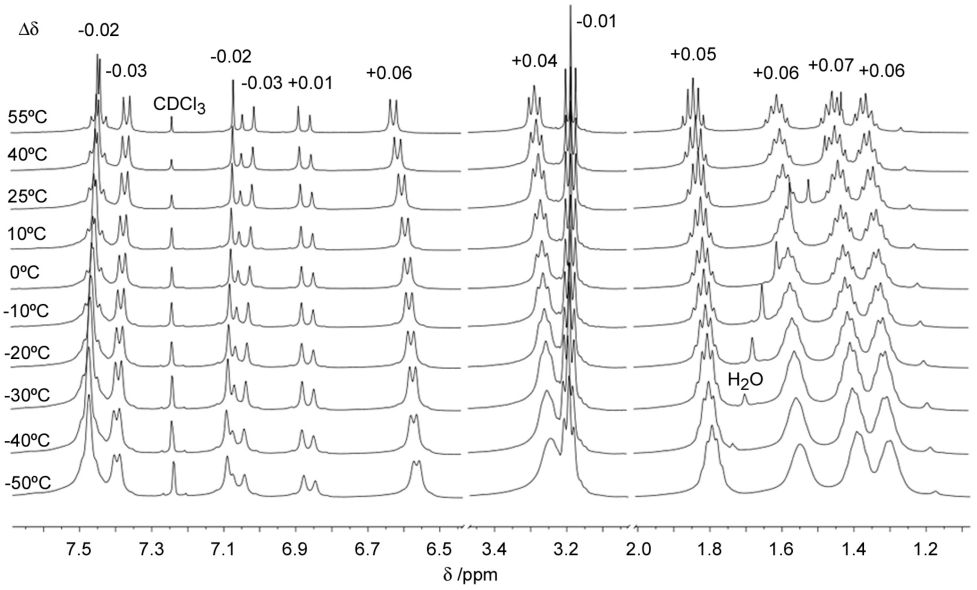

Figure 10. ^{1}H NMR spectra of a 0.02 M DSSI solution in $CDCl_3$ at indicated temperatures.

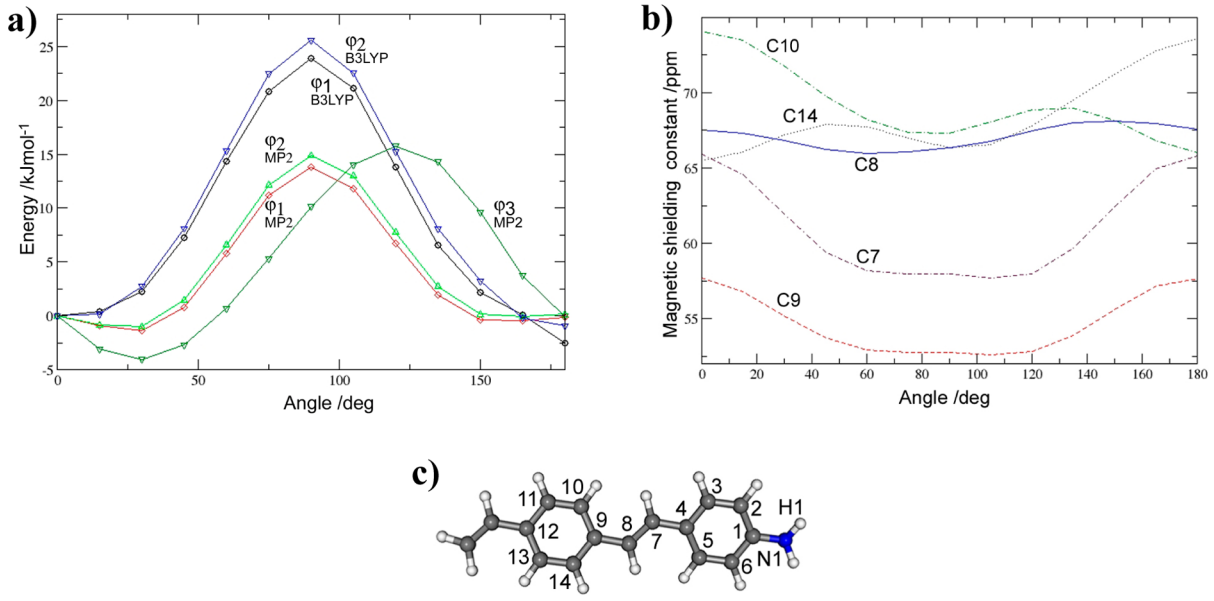

Figure 11. (a) Energy as a function of dihedral angle calculated for φ_1(10, 9, 8, 7), φ_2(8, 7, 4, 5), and φ_3(2, 1, N1, H1) at MP2/3-21G(d) and B3LYP/6-31G(d,p) levels. (b) ^{13}C nuclear magnetic shielding constant calculated for the MP2/3-21G(d) structures as a function of the dihedral angle φ_1(10, 9, 8, 7) of the model presented in c.

Figure 10, we saw that in the range of temperatures from −30 °C to +55 °C the chemical shift of all the backbone carbon atoms of DSSI undergo positive $\Delta\delta$ values. In terms of magnetic shielding constant, this means they undergo negative $\Delta\sigma$ values (δ and σ have opposite signs). The curves in Figure 11b reveal that $\Delta\sigma$ is negative for all the carbon atoms considered in this analysis only when the dihedral angle changes from around 45 degrees to 60 degrees and from around 135 to 105 degrees. This result suggests that with the increase in temperature from −30 °C to +55 °C the backbone dihedral angle varies from close to 45 degrees to close to 60 degrees or from close to 135 to close to 105 degrees. Thus, the average conformation of the COs at higher temperatures is more twisted, that is, displays a more perpendicular arrangement of the conjugated framework components. This structural preference confirms the observed blue shift in PL at higher temperatures.

DISCUSSION

CO/Solvent Interaction. Following on from earlier work on trimeric *p*-phenylenevinylene oligomers,[21,25,26] our initial goal was to study backbone conformational relaxation in the excited singlet states of three oligomers DSBI, DSSI, and COE5I in different solvents. NMR spectral measurements coupled with DFT, MP2, and semiempirical calculations reveal that these oligomers have a rich conformational behavior. However, both fluorescence spectral and lifetime measurements show that with these three oligomers this relaxation process is much faster than with the other trimeric *p*-phenylenevinylenes. Previous non-adiabatic excited-state molecular dynamics modeling on

dx.doi.org/10.1021/jp406048g | J. Phys. Chem. C 2013, 117, 18353−18366

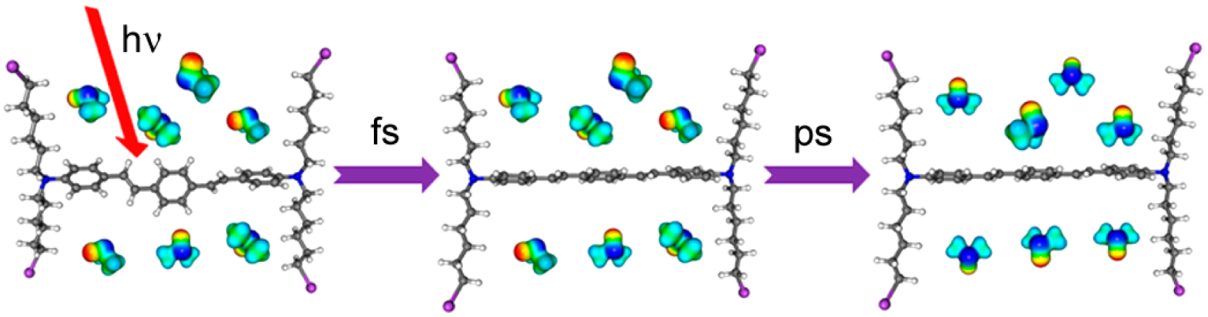

Figure 12. Schematic representation of the conformation relaxation and the solvent relaxation upon excitation.

distyrylbenzene (equivalent to DSBI) in its lowest excited singlet state suggests that backbone torsional relaxation occurs in about 100 fs.[33] The difference in behavior between the oligomers in the present study and the previously studied distyrylbenzene oligomers[21,25,26] must result from the latter containing substituents on the aromatic rings. These are likely to enhance coupling between any conformational changes on the oligomers and the solvent, whereas with DSBI and the other oligomers studied here, relatively pure torsional dynamics of the backbone is expected. However, with the donor−acceptor−donor oligomers DSBI, DSSI, and COE5I, another process is seen in the fluorescence decays observed on a time scale of tens of picoseconds in solvents, such as toluene and DMF. Previous studies showing local solvation and specific interactions between the various pairwise interactions involving backbone, side chain, and solvent are important with conjugated polymers.[35,36] In general, the reorganization energies and the time-dependent solvation response are described assuming a dielectric continuum. Although this assumption might be valid in some cases, it is also true that there are several examples where this assumption is inadequate. One example is the case of coumarin C153 in benzene, where time-dependent emission shifts were observed. This behavior was assigned to solute−solvent interactions.[37] Solvation effects were also observed in many conjugated polymers. In fact, 2,7-dibromo-9,9-dioctylfluorene in chlorinated alkanes is the subject of attractive interactions between these solvents and the polymer backbone leading to the formation of solvated species[38] as has also been observed with other aromatic molecules and halomethanes.[39] In THF, the polymer shows the formation of polymer−polymer $\pi-\pi$ complex, whereas in toluene (aromatic solvent), the formation of polymer−solvent complex is more likely to occur.[40,41] In THF, MCH, and cyclohexane, there is little interaction between the solvent and the backbone as the solvent mainly interacts with the side chains.

Thus, we believe that in our systems the interplay between the dialkylamino-*p*-phenylenevinylene group and the solvent determines the photophysical behavior of these oligomers in solution. The fact that the PL maxima in DMF, chloroform, and DMSO do not fit the Onsager relationship (see the SI) but can be fitted with a Lippert−Mataga plot shows the importance of specific solvent interactions with these systems. From the fluorescence decays, we can distinguish two decay patterns. In alkenes, the decays are monoexponential, while in toluene, THF and DMF are biexponential with a fast rise time at longer emission wavelengths. *n*-Hexane, *n*-hexadecane, and MCH are poor solvents for the *p*-phenylenevinylene groups, and the solvent−oligomer interaction occurs mainly with the terminal alkyl chains. The oligomer backbone adopts a well-defined conformation and decays with its natural decay time. Toluene, as mentioned above, is an aromatic solvent and is a good solvent for the *p*-PV groups. The occurrence of $\pi-\pi$ interactions is expected to lead to the formation of oligomer−solvent complex, and the rise time at longer emission wavelengths might result from the solvent relaxation in the excited state. The fast component observed in DMF is also expected to be associated with solvent relaxation. The excited-state pathways of DSBI following photoexcitation are summarized in Figure 12.

CONCLUSIONS

We have performed photophysical characterization of three *p*-phenylenevinylene oligomers, with different chain lengths, capped at each end with nitrogen-bound hexyl iodide pendant groups. The three oligomers displayed similar sensitivities to the solvent and temperature, and their photophysical behavior seems to be governed by ICT and specific chromophore/solvent interactions. Theoretical calculations confirmed that these phenylenevinylene cores do not adopt a fully planar conformation, and their conformation is shown to be temperature dependent. The effect of temperature was also studied through NMR spectroscopy; both ^{1}H and ^{13}C NMR spectra changed with temperature and showed changes in the different population states as the temperature increased which is in agreement with the changes observed in the photoluminescence spectra.

In contrast to substituted *p*-phenylenevinylene oligomers, where conformational relaxation occurs in the tens of picosecond time range, with the three oligomers investigated, an ultrafast backbone conformational relaxation is suggested. However, in some solvents, a component with a lifetime of tens of picoseconds is seen and is attributed to solvent reorientation around the conformationally relaxed excited oligomer. These results show that it is possible to decouple conformational relaxation and solvent reorientation in *p*-phenylenevinylene oligomers by appropriate structural modification. Because conformational relaxation enhances nonradiative decay of excited states, control of this is expected to improve photoluminescence yields in these systems and, hence, device properties. It seems likely that the same concept can be extended to other conjugated oligomers and polymers.

MATERIALS, METHODS, AND TECHNIQUES

Materials. The syntheses of the three oligomers DSBNI, DSSNI, and COE5NI presented in Scheme 1 were, respectively, reported in refs 27, 42, and 43. The concentration of the oligomers was kept in the 1−5 μM range. Chloroform (spectroscopic grade) was purchased from Sigma-Aldrich. Toluene, tetrahydrofuran (THF), dimethylformamide (DMF), decane, and hexadecane (Spectranal) were purchased from

dx.doi.org/10.1021/jp406048g | J. Phys. Chem. C 2013, 117, 18353−18366

Riedel-deHaën. Methylcyclohexane (MCH), dodecane, and tetradecane were purchased for spectroscopy from ACROS. Hexane and dimethylsulfoxide (DMSO) of spectroscopic grade were from LAB-SCAN. The solvents were free of fluorescent impurities upon excitation in the 380−450 nm range. Alkanes are poor solvents for the *p*-phenylenevinylene (*p*-PV) oligomers, and the solvent−oligomer interaction occurs mainly with the terminal alkyl chains. Solubility issues become more important with increasing the number of *p*-PV groups. This is also observed in polar solvents, such as DMSO and DMF. In contrast, toluene and THF are good solvents for the *p*-PV groups of the three oligomers studied.

Absorption Spectra. The absorption spectra were recorded on a Shimadzu UV-2100 spectrophotometer; all spectra were acquired with a minimum resolution of 0.2 nm.

Steady-State Fluorescence. The fluorescence spectra were recorded with a Horiba-Jobin-Ivon SPEX Fluorog 3-22 spectrometer and were corrected for the instrumental response. The fluorolog consists of a modular spectrofluorimeter with double grating excitation (range 200−950 nm, optimized in the UV and with an angle blazed at 330 nm) and emission (range 200−950 nm, optimized in the visible and with an angle blazed at 500 nm) monochromators. The bandpass for excitation and emission is 0−15 nm (values that are continuously adjustable from computer Datamax/32 software), and the wavelength accuracy is ±0.5 nm. The excitation source consists of an ozone-free 450 W xenon lamp, and the emission detector is a Hamamatsu R928 Photomultiplier (200−900 nm range) cooled with a Products for Research thermoelectric refrigerated chamber (model PC177CE005) or a Hamamatsu R5509-42 (900−1400 nm range) cooled to 193 K in a liquid nitrogen chamber (Products for Research model PC176TSCE-005) and with a photodiode as the reference detector.

Flash Photolysis. The experimental setup used to obtain triplet state absorption spectra and quantum yields involves an Applied Photophysics laser flash photolysis apparatus pumped by a Nd:YAG laser (Spectra Physics). Transient spectra were obtained by monitoring the optical density change at intervals of 10 nm over the 300−700 nm range and by averaging at least 10 decays at each wavelength. Second-order kinetics was observed for the decay of the lowest triplet state. Excitation was at 355 nm with an unfocused beam. Special care was taken in determining triplet yields to have optically matched dilute solutions (abs ≈ 0.2−0.3 in a 10 mm square cell) and low laser energy (2 mJ) to avoid multiphoton and triplet−triplet (T−T) annihilation effects. The triplet molar absorption coefficients were determined by the singlet depletion technique according to the well-known relationship

$$\varepsilon_T = \frac{(\varepsilon_S)(\Delta OD_T)}{(\Delta OD_S)}$$

where both ΔOD_S and ΔOD_T were obtained from the triplet transient absorption spectra, and triplet formation quantum yields were derived from these and actinometry with benzophenone. The intersystem-crossing yields (ϕ_T) for the compounds were obtained by comparing the ΔOD at 530 nm of benzene solutions of benzophenone (standard) optically matched (at the laser excitation wavelength) and of the compound using the following equation:

$$\phi_T^{\text{sample}} = \frac{\varepsilon_{TT}^{\text{benzophenone}}}{\varepsilon_{TT}^{\text{sample}}} \frac{\Delta OD_{max}^{\text{sample}}}{\Delta OD_{max}^{\text{benzophenone}}} \phi_T^{\text{benzophenone}}$$

with $\varepsilon_{TT}^{\text{benzophenone}} = 7200\ M^{-1}\ cm^{-1}$ and $\phi_T^{\text{benzophenone}} = 1$.

Room-temperature singlet oxygen phosphorescence was detected at 1270 nm with a Hamamatsu R5509-42 photomultiplier cooled to 193 K in a liquid nitrogen chamber (Products for Research model PC176TSCE-005) after laser excitation at 355 nm in an adapted Applied Photophysics flash kinetic spectrometer.[44] The sensitized phosphorescence emission spectra of singlet oxygen from optically matched solutions of the samples and that of reference were obtained in identical experimental conditions. The singlet oxygen formation quantum yield was then determined by applying the following equation:

$$\phi_\Delta^{\text{sample}} = \frac{\int I(\lambda)^{\text{sample}} d\lambda}{\int I(\lambda)^{\text{ref}} d\lambda} \phi_\Delta^{\text{ref}}$$

where $\int I(\lambda)^{\text{sample}} d\lambda$ and $\int I(\lambda)^{\text{ref}} d\lambda$ are, respectively, the integrated area under the sensitized emission spectra of singlet oxygen of the sample solution and that of the reference solution, and ϕ_Δ^{ref} is the singlet oxygen formation quantum yield of the reference compound, that is, of 1H-Phenalen-1-one in benzene ($\phi_\Delta = 0.93$).[45]

Time-Resolved Fluorescence. Fluorescence decays were measured using the time-correlated single-photon counting (TCSPC) and fluorescence upconversion (FUC) techniques. The TCSPC equipment was previously described:[18] the excitation was provided by a Millennia Xs/Tsunami lasers system from Spectra Physics, operating at 82 MHz, and was frequency-doubled. The sample emission was collected at the magic angle (Glan-Thompson polarizer), was passed through a monochromator (Jobin-Yvon H20 Vis), and was detected with a microchannel plate photomultiplier (Hamamatsu R3809u-50). The full width at half-maximum (fwhm) of the instrumental response (obtained with a scattering Ludox solution) is ca. 18 ps with 814 fs/channel resolution.

For FUC measurements, a Millennia Xs laser was used to pump a CDP Systems Inc. setup composed of a fs-Ti:sapphire laser (TISSA-100), a CDP 2015 frequency doubler/tripler, and a Femtosecond Optically Gated Fluorescence Kinetic Measurement System (FOG-100).[46] The polarization of the (pump) excitation pulses (ca. 200 fs fwhm) was set at the magic angle with respect to the gate pulse. The sample was placed in a rotating cell constituted by two 37.5 mm diameter quartz disks at 1 mm distance. The fluorescence of the sample and the gate beam were overlapped on a nonlinear crystal, and the upconverted photons were passed through a CDP2022D double monochromator and were detected with a photon-counting photomultiplier tube (PMT). The excitation pulse instrumental response function (IRF) was collected with the Raman scatter of water. All fluorescence decays were deconvoluted from the IRF using the Sand program.[47]

NMR Methodology. The DSSI samples for the NMR experiments were prepared by dissolving weighed amounts of the polymer in chloroform-*d* or toluene-d_8 and were kept protected from light. Chloroform-*d* (99.8 atom % ^2H) and toluene-d_8 (99 atom % ^2H) were purchased from Sigma-Aldrich, Inc., Germany. The ^1H and ^{13}C NMR spectra were recorded on a Varian VNMRS 600 MHz spectrometer (at 599.72 and 150.80 MHz, respectively). The signals of $CDCl_3$ at δ = 7.27 ppm and of toluene at δ = 2.09 ppm, relative to tetramethylsilane (TMS), were used as internal references for ^1H, while the ^{13}C triplet of $CDCl_3$ centered at δ = 77.23 ppm and the heptet of toluene centered at δ = 20.40 ppm were used as internal references for ^{13}C. The COSY (correlation spectroscopy), HETCOR

dx.doi.org/10.1021/jp406048g | J. Phys. Chem. C 2013, 117, 18353−18366

(heteronuclear correlation), DEPT (distortionless enhancement by polarization transfer), and ROESY (rotating frame Overhause effect spectroscopy) spectra were recorded on the same spectrometer. For the variable temperature studies, the samples were allowed to attain thermal equilibrium before acquiring the spectra.

Computational Details. The DFT calculations employed the B3LYP (Becke three-parameter Lee−Yang−Parr exchange correlation)[48,49] functional and the 6-31G(d,p) standard basis sets for the expansion of the Kohn−Sham orbitals, and the geometry optimizations at the MP2 level employed the 3-21G(d) standard basis sets. For the oligomers, the $C_6H_{12}I$ substituents at the nitrogen atoms were replaced by ethyl moieties to reduce the computation time. At the final equilibrium geometries with minimum energy, the gradient was 1×10^{-05} hartree bohr^{-1}. The MP2 and DFT geometry optimizations were performed using the GAMESS code.[4] The magnetic nuclear shielding constants were computed at the B3LYP/GIAO (gauge-including atomic orbital method) level using the NWCHEM[50,51] program, the 6-31G(d,p) basis sets, and a fine integration grid (FINE option). ^{13}C relative chemical shifts (δ) are given with respect to the absolute shielding values (σ) of tetramethylsilane (TMS) obtained at the same computational level ($\delta = \sigma_{ref} - \sigma$). The effects of the torsion angle on the energy and on the ^{13}C NMR chemical shifts of a model system were analyzed at the B3LYP/6-31G(d,p) and MP2/3-21G(d) levels starting from the optimized structures of the model and varying the dihedral angles by 15° steps. The structures were relaxed at each torsion angle, and for each structure, the nuclear shieldings were computed and were converted into relative chemical shifts as indicated above. The semiempirical quantum chemistry calculations were performed with the MOPAC2007[52] system of programs using the PM6[53] Hamiltonian and the EF routine.

Conformational aspects of single molecules of oligomers in a box of DMSO solvent were also studied by MD. All simulations were carried out in the NpT ensemble and under periodic boundary conditions resorting to the GROMACS package, version 4.5.4.[54] Topologies for the DSBI, DSSI, and COE5I residues were generated by the PRODRG server,[55] while DMSO was used as made available in the original GROMOS 96 43a1 force field.[56] A standard time step of 2 fs was used for both the equilibration and the production runs. Nonbonded interactions were computed on the basis of a neighbor list updated every 10 steps. Long-range electrostatics was computed using the particle mesh Ewald (PME) method. For Lennard-Jones energies, a cutoff of 1.4 nm was applied. Temperature (273 K, 298 K) and pressure (1 bar) were coupled to the Berendsen external baths with coupling constants of 0.1 and 0.5 ps, respectively. Each system was first subjected to an energy minimization step and then was left to evolve up to 60 ns. The last 30 ns of production runs was subsequently subjected to standard analysis, such as distances, angles, and radial distribution functions. MD trajectories were visualized, and configuration images were extracted using the VMD 1.8.6 software.[57]

■ ASSOCIATED CONTENT

Supporting Information

HOMO and LUMO orbitals calculated at the B3LYP/6-31G(d,p) level; dependence of the wavenumber shift on the $E_T(30)$ values, for DSBI, DSSNI and COE5I, in different solvents; fluorescence decays; semiempirical PM6 optimized structures of the DSBI, DSSI and COE5I; end-to-end distances obtained between the N atoms for DSBI, DSSI and COE5I molecules as extracted from the MD simulations at 273 K and 298 K; comparison between the ^{13}C NMR experimental chemical shifts of the tetramer DSSI in $CDCl_3$ and toluene-d_8 at 298.15 K; normalized PL and excitation spectra of DSSI in chloroform as a function of the temperature; Arrhenius plots of (τ_1^{-1}) for DSBI, DSSI and COE5I toluene and chloroform. This material is available free of charge via the Internet at http://pubs.acs.org.

■ AUTHOR INFORMATION

Corresponding Author

*E-mail: tcosta@qui.uc.pt.

Notes

The authors declare no competing financial interest.

■ ACKNOWLEDGMENTS

Portuguese Science Foundation (FCT) is acknowledged for the postdoc grants SFRH/BPD/47181/2008 (T.C.), SFRH/BPD/26415/2006 (L.L.G.J.), and SFRH/BPD/82125/2011 (J.A.S.A.). FCT is also acknowledged for funding through projects no. PTDC/QUI-QUI/101442/2008 (COMPETE:F-COMP-01-0124-FEDER-010831). L.L.G.J. and J.A.S.A. also thank the generous allocation of computational time in Milipeia cluster, LCA, University of Coimbra, Portugal. Work at UCSB has been supported through the National Science Foundation (DMR 1005546).

■ REFERENCES

(1) Egbe, D. A. M.; Neugebauer, H.; Sariciftci, N. S. Alkoxy-Substituted Poly(Arylene-Ethynylene)-*alt*-Poly(Arylene-Vinylene)s: Synthesis, Electroluminescence and Photovoltaic Applications. *J. Mater. Chem.* **2011**, *21*, 1338−1349.

(2) Evenson, S. J.; Mumm, M. J.; Pokhodnya, K. I.; Rasmussen, S. C. Highly Fluorescent Dithieno[3,2-*b*:2 ′,3 ′-*d*]pyrrole-Based Materials: Synthesis, Characterization, and OLED Device Applications. *Macromolecules* **2011**, *44*, 835−841.

(3) Murphy, C. B.; Zhang, Y.; Troxler, T.; Ferry, V.; Martin, J. J.; Jones, W. E. Probing Forster and Dexter Energy-Transfer Mechanisms in Fluorescent Conjugated Polymer Chemosensors. *J. Phys. Chem. B* **2004**, *108*, 1537−1543.

(4) Schmidt, M. W.; Baldridge, K. K.; Boatz, J. A.; Elbert, S. T.; Gordon, M. S.; Jensen, J. H.; Koseki, S.; Matsunaga, N.; Nguyen, K. A.; Su, S. J.; Windus, T. L.; Dupuis, M.; Montgomery, J. A. General Atomic and Molecular Electronic Structure System. *J. Comput. Chem.* **1993**, *14*, 1347−1363.

(5) Pauly, A. C.; Theato, P. Toward Photopatternable Thin Film Optical Sensors Utilizing Reactive Polyphenylacetylenes. *Macromol. Rapid Commun.* **2013**, *34*, 516−521.

(6) Brédas, J.-L.; Beljonne, D.; Coropceanu, V.; Cornil, J. Charge-Transfer And Energy-Transfer Processes In Pi-Conjugated Oligomers And Polymers: A Molecular Picture. *Chem. Rev.* **2004**, *104*, 4971−5003.

(7) Duarte, A.; Pu, K.-Y.; Liu, B.; Bazan, G. C. Recent Advances in Conjugated Polyelectrolytes for Emerging Optoelectronic Applications. *Chem. Mater.* **2011**, *23*, 501−515.

(8) Pinto, M. R.; Schanze, K. S. Conjugated Polyelectrolytes: Synthesis and Applications. *Synthesis* **2002**, *9*, 1293−1309.

(9) Jiang, H.; Taranekar, P.; Reynolds, J. R.; Schanze, K. S. Conjugated Polyelectrolytes: Synthesis, Photophysics, and Applications. *Angew. Chem., Int. Ed.* **2009**, *48*, 4300−4316.

(10) Garcia, A.; Nguyen, T.-Q. Effect of Aggregation on the Optical and Charge Transport Properties of an Anionic Conjugated Polyelectrolyte. *J. Phys. Chem. C* **2008**, *112*, 7054−7061.

(11) Knaapila, M.; Garamus, V. M.; Dias, F. B.; Almásy, L.; Galbrecht, F.; Charas, A.; Morgado, J.; Burrows, H. D.; Scherf, U.; Monkman, A. P. Influence of Solvent Quality on the Self-Organization of Archetypical Hairy Rods−Branched and Linear Side Chain Polyfluorenes: Rodlike

Chains versus "Beta-Sheets" in Solution. *Macromolecules* **2006**, *39*, 6505−6512.
(12) Burroughes, J. H.; Bradley, D. D. C.; Brown, A. R.; Marks, R. N.; Mackay, K.; Friend, R. H.; Burns, P. L.; Holmes, A. B. Light-Emitting Diodes Based on Conjugated Polymers. *Nature* **1990**, *347*, 539−541.
(13) Scherf, U. Ladder-Type Materials. *J. Mater. Chem.* **1999**, *9*, 1853−1864.
(14) Xu, Z. H.; Tsai, H. H.; Wang, H. L. Solvent Polarity Effect on Chain Conformation, Film Morphology, and Optical Properties of a Water-Soluble Conjugated Polymer. *J. Phys. Chem. B* **2010**, *114*, 11746−11752.
(15) Köhler, A.; Hoffman, S. T.; Bässler, H. An Order−Disorder Transition in the Conjugated Polymer MEH-PPV. *J. Am. Chem. Soc.* **2012**, *134*, 11594−11601.
(16) Feist, F. A.; Basché, T. The Folding of Individual Conjugated Polymer Chains during Annealing. *Angew. Chem., Int. Ed.* **2011**, *50*, 5256−5257.
(17) Pond, S. J. K.; Rumi, M.; Levin, M. D.; Parker, T. C.; Beljonne, D.; Day, M. W.; Brédas, J.-L.; Marder, S. M.; Perry, J. W. One- and Two-Photon Spectroscopy of Donor−Acceptor−Donor Distyrylbenzene Derivatives: Effect of Cyano Substitution and Distortion from Planarity. *J. Phys. Chem. A* **2012**, *106*, 11470−11480.
(18) Seixas de Melo, J. S.; Pina, J.; Burrows, H. D.; Brocke, S.; Herzog, O.; Thorn-Csányi, E. The Effect of Substitution and Isomeric Imperfection on the Photophysical Behaviour of *p*-Phenylenevinylene Trimers. *Chem. Phys. Lett.* **2004**, *388*, 236−241.
(19) Burrows, H. D.; Narwark, O.; Peetz, R.; Thorn-Csányi, E.; Monkman, A. P.; Hamblett, I.; Navaratnam, S. Mechanistic Studies on the Photodegradation of 2,5-dialkyloxyl-Substituted Para-Phenylenevinylene Oligomers by Singlet Oxygen. *Photochem. Photobiol. Sci.* **2010**, *9*, 942−948.
(20) Pina, J.; Seixas de Melo, J. S.; Burrows, H. D.; Maçanita, A. L.; Galbrecht, F.; Bunnagel, T. Scherf, U. Alternating Binaphthyl−Thiophene Copolymers: Synthesis, Spectroscopy, and Photophysics and Their Relevance to the Question of Energy Migration versus Conformational Relaxation. *Macromolecules* **2009**, *42*, 1710−1719.
(21) Seixas de Melo, J. S.; Pina, J.; Burrows, H. D.; Di Paolo, R. E.; Maçanita, A. L. Electronic Spectral and Photophysical Properties of Some p-Phenylenevinylene Oligomers in Solution and Thin Films. *Chem. Phys.* **2006**, *330*, 449−456.
(22) Burrows, H. D.; Seixas de Melo, J.; Serpa, C.; Arnaut, L. G.; Monkman, A. P.; Hamblett, I. Navaratnam, S. S1 ∼ >T1 Intersystem Crossing in π-Conjugated Organic Polymers. *J. Chem. Phys.* **2001**, *115*, 9601−9606.
(23) Dogariu, A.; Vacar, D.; Heeger, A. J. Picosecond Time-Resolved Spectroscopy of the Excited State in a Soluble Derivative of Poly(Phenylene Vinylene): Origin of the Bimolecular Decay. *Phys. Rev. B* **1998**, *58*, 10218−10224.
(24) Di Paolo, R. E.; Burrows, H. D.; Morgado, J.; Maçanita, A. L. Photodynamics of a PV Trimer in High-Viscosity Solvents and in PMMA Films: A New Insight into Energy Transfer versus Conformational Relaxation in Conjugated Polymers. *ChemPhysChem* **2009**, *10*, 448−454.
(25) Di Paolo, R. E.; Gigante, B.; Esteves, M. A.; Pires, N.; Lameiro, C. S. M. H.; Seixas de Melo, J.; Burrows, H. D. Maçanita, A. L. Picosecond Structural Relaxation of Abietic Acid Based Amine End Capped Para-Phenylenevinylene Trimers in Solution. *ChemPhysChem* **2008**, *9*, 2214−2220.
(26) Di Paolo, R. E.; Seixas de Melo, J. S.; Pina, J.; Burrows, H. D.; Morgado, J.; Maçanita, A. L. Conformational Relaxation of p-Phenylenevinylene Trimers in Solution Studied by Picosecond Time-Resolved Fluorescence. *Chem. Phys. Chem.* **2007**, *8*, 2657−2664.
(27) Woo, H. Y.; Liu, B.; Kohler, B.; Korystov, D.; Mikhailovsky, A.; Bazan, G. C. Solvent Effects on the Two-Photon Absorption of Distyrylbenzene Chromophores. *J. Am. Chem. Soc.* **2005**, *127*, 14721−14729.
(28) Lakowicz, J. R. *Principles of Fluorescence Spectroscopy*, 3rd ed.; Springer: New York, 2006.
(29) Reichardt, C. Solvatochromic Dyes as Solvent Polarity Indicators. *Chem. Rev.* **1994**, *94*, 2319−2358.
(30) Mukamel, S. Quantum Chemistry: A Lightning-Fast Change. *Nat. Phys.* **2012**, *2012*, 179−180.
(31) Clark, J.; Nelson, T.; Tretiak, S.; Cirmi, G.; Lanzani, G. Femtosecond Torsional Relaxation. *Nat. Phys.* **2012**, *8*, 225−231.
(32) Galvão, A. M.; Di Paolo, R. E.; Maçanita, A. L.; Naqvi, R. Model for Conformational Relaxation of Flexible Conjugated Polymers: Application to p-Phenylenevinylene Trimers in Nonpolar Solvents. *Chem. Phys. Chem.* **2013**, *14*, 583−590.
(33) Nelson, T.; Fernandez-Alberti, S.; Chernyak, V.; Roitberg, A. E.; Tretiak, S. Nonadiabatic Excited-State Molecular Dynamics Modeling of Photoinduced Dynamics in Conjugated Molecules. *J. Phys. Chem. B* **2011**, *115*, 5402−5414.
(34) Justino, L. L. G.; Ramos, M. L.; Abreu, P. E.; Carvalho, R. A.; Sobral, A. J. F. N.; Scherf, U.; Burrows, H. D. Conformational Studies of Poly(9,9-dialkylfluorene)s in Solution Using NMR Spectroscopy and Density Functional Theory Calculations. *J. Phys. Chem. B* **2009**, *113*, 11808−11821.
(35) Burrows, H. D.; Fonseca, S. M.; Silva, C. L.; Pais, A. A. C. C.; Tapia, M. J.; Pradhan, S.; Scherf, U. Aggregation of the Hairy Rod Conjugated Polyelectrolyte Poly{1,4-phenylene-[9,9-bis(4-phenoxybutylsulfonate)]fluorene-2,7-diyl} in Aqueous Solution: An Experimental and Molecular Modelling Study. *Phys. Chem. Chem. Phys.* **2008**, *10*, 4420−4428.
(36) Justino, L. L. G.; Ramos, M. L.; Knaapila, M.; Marques, A. T.; Kudla, C. J.; Scherf, U.; Almásy, L.; Schweins, R.; Burrows, H. D.; Monkman, A. P. Gel Formation and Interpolymer Alkyl Chain Interactions with Poly(9,9-dioctylfluorene-2,7-diyl) (PFO) in Toluene Solution: Results from NMR, SANS, DFT, and Semiempirical Calculations and Their Implications for PFO β-Phase Formation. *Macromolecules* **2011**, *44*, 334−343.
(37) Reynolds, L.; Gardecki, J. A.; Frankland, S. J. V.; Horng, M. L.; Maroncelli, M. Dipole Solvation in Nondipolar Solvents: Experimental Studies of Reorganization Energies and Solvation Dynamics. *J. Phys. Chem.* **1996**, *100*, 10337−10354.
(38) Leclerc, M.; Ranger, M.; Bélanger-Gariépy, F. 2,7-Dibromo-9,9-dioctylfluorene−Chloroform (1/0.25). *Acta Crystallogr., Sect. C* **1998**, *54*, 799−801.
(39) Davis, K. M. C.; Farmer, M. F. Charge-Transfer Complexes. Part V. Nature of the Interaction of Halogenomethanes and Aromatic Hydrocarbons. *J. Chem. Soc. B* **1968**, 859−862.
(40) Rahman, M. H.; Chen, C.-Y.; Liao, S.-C.; Chen, H.-L.; Tsao, C.-S.; Chen, J.-H.; Liao, J.-L.; Ivanov, V. A.; Chen, S.-A. Segmental Alignment in the Aggregate Domains of Poly(9,9-dioctylfluorene) in Semidilute Solution. *Macromolecules* **2007**, *40*, 6572−6578.
(41) Traiphol, R.; Srikhirin, T.; Kerdcharoen, T.; Osotchan, T.; Scharnagl, N.; Willumeit, R. Influences of Local Polymer−Solvent π−π-Interaction on Dynamics of Phenyl Ring Rotation and Its Role on Photophysics of Conjugated Polymer. *Eur. Polym. J.* **2007**, *43*, 478−487.
(42) Garner, L. E.; Park, J.; Dyar, S. M.; Chworos, A.; Sumner, J. J.; Bazan, G. C. Modification of the Optoelectronic Properties of Membranes via Insertion of Amphiphilic Phenylenevinylene Oligoelectrolytes. *J. Am. Chem. Soc.* **2010**, *132*, 10042−10052.
(43) Hou, H.; Chen, X.; Thomas, A. W.; Catania, C.; Kirchhofer, N. D.; Garner, L. E.; Han, A.; Bazan, G. C. Conjugated Oligoelectrolytes Increase Power Generation in *E. coli* Microbial Fuel Cells. *Adv. Mater.* **2013**, *25*, 1593−1597.
(44) Pina, J.; Seixas de Melo, J. A Comprehensive Investigation of the Electronic Spectral and Photophysical Properties of Conjugated Naphthalene−Thiophene Oligomers. *Phys. Chem. Chem. Phys.* **2009**, *11*, 8706−8713.
(45) Flors, C.; Nonell, S. On the Phosphorescence of 1H-Phenalen-1-one. *Helv. Chim. Acta* **2001**, *84*, 2533−2539.
(46) Ferreira, B.; Silva, P. F.; Seixas de Melo, J. S.; Pina, J. Maçanita, A. L. Excited-State Dynamics and Self-Organization of Poly(3-Hexylthiophene) (P3HT) in Solution and Thin Films. *J. Phys. Chem. B* **2012**, *116*, 2347−2355.

(47) Striker, G.; Subramaniam, V.; Seidel, C. A. M.; Volkmer, A. *J. Phys. Chem. B* **1999**, *103*, 8612−8617.
(48) Becke, A. D. Density-Functional Thermochemistry. III. The Role of Exact Exchange. *J. Chem. Phys.* **1993**, *98*, 5648−5652.
(49) Lee, C.; Yang, W.; Parr, R. G. Development of the Colle-Salvetti Correlation-Energy Formula into a Functional of the Electron Density. *Phys. Rev. B* **1988**, *37*, 785−789.
(50) Kendall, R. A.; Apra, E.; Bernholdt, D. E.; Bylaska, E. J.; Dupuis, M.; Fann, G. I.; Harrison, R. J.; Ju, J.; Nichols, J. A.; Nieplocha, J.; Straatsma, T. P.; Windus, T. L.; Wong, A. T. High Performance Computational Chemistry: An Overview of NWChem a Distributed Parallel Application. *Comput. Phys. Commun.* **2000**, *128*, 260−283.
(51) Bylaska, E. J.; de Jong, W. A.; Govind, N.; Kowalski, K.; Straatsma, T. P.; Valiev, M.; Wang, D.; Apra, E.; Windus, T. L.; Hammond, J.; Nichols, P.; Hirata, S.; Hackler, M. T.; Zhao, Y.; Fan, P.-D.; Harrison, R. J.; Dupuis, M.; Smith, D. M. A.; Nieplocha, J.; Tipparaju, V.; Krishnan, M.; Wu, Q.; Van Voorhis, T.; Auer, A. A.; Nooijen, M.; Brown, E.; Cisneros, G.; Fann, G. I.; Fruchtl, H.; Garza, J.; Hirao, K.; Kendall, R.; Nichols, J. A.; Tsemekhman, K.; Wolinski, K.; Anchell, J.; Bernholdt, D.; Borowski, P.; Clark, T.; Clerc, D.; Dachsel, H.; Deegan, M.; Dyall, K.; Elwood, D.; Glendening, E.; Gutowski, M.; Hess, A.; Jaffe, J.; Johnson, B.; Ju, J.; Kobayashi, R.; Kutteh, R.; Lin, Z.; Littlefield, R.; Long, X.; Meng, B.; Nakajima, T.; Niu, S.; Pollack, L.; Rosing, M.; Sandrone, G.; Stave, M.; Taylor, H.; Thomas, G.; van Lenthe, J.; Wong, A.; Zhang, Z. *NWChem, A Computational Chemistry Package for Parallel Computers*; Pacific Northwest National Laboratory: Richland, Washington, 2007.
(52) *MOPAC2007*, version 8.087L; James J. P. Stewart, Stewart Computational Chemistry: Colorado Springs, CO, 2007; HTTP://OpenMOPAC.net.
(53) Stewart, J. J. Optimization of Parameters for Semiempirical Methods V: Modification of NDDO Approximations and Application to 70 elements. *J. Mol. Model.* **2007**, *13*, 1173−1213.
(54) Hess, B.; Kutzner, C.; Spoel, D. v. d.; Lindahl, E. GROMACS 4: Algorithms for Highly Efficient, Load-Balanced, and Scalable Molecular Simulation. *J. Chem. Theory. Comput.* **2008**, *4*, 435−447.
(55) Schuttelkopf, A. W.; Aalten, D. M. F. v. PRODRG: A Tool for High-Throughput Crystallography of Protein±Ligand Complexes. *Acta Crystallogr. D* **2004**, *60*, 1355−1363.
(56) Schuler, L. D.; Daura, X.; Gunsteren, W. F. V. An Improved GROMOS96 Force Field for Aliphatic Hydrocarbons in the Condensed Phase. *J. Comput. Chem.* **2001**, *22*, 1205−1218.
(57) Humphrey, W.; Dalke, A.; Schulten, K. VMD: Visual Molecular Dynamics. *J. Molec. Graphics* **1996**, *14*, 33−38.
(58) Montalti, M.; Credi, A.; Luca, P. Gandolfi, M. T., *Handbook of Photochemistry*, 3rd ed.; Taylor & Francis Inc.: New York, 2006.